PAPER • OPEN ACCESS

Attosecond transient absorption of argon atoms in the vacuum ultraviolet region: line energy shifts versus coherent population transfer

To cite this article: Wei Cao *et al* 2016 *New J. Phys.* **18** 013041

New Journal of Physics
The open access journal at the forefront of physics

Deutsche Physikalische Gesellschaft DPG
IOP Institute of Physics

Published in partnership with: Deutsche Physikalische Gesellschaft and the Institute of Physics

OPEN ACCESS

RECEIVED
18 August 2015

REVISED
8 December 2015

ACCEPTED FOR PUBLICATION
9 December 2015

PUBLISHED
18 January 2016

PAPER

Attosecond transient absorption of argon atoms in the vacuum ultraviolet region: line energy shifts versus coherent population transfer

Wei Cao[1,2,3], **Erika R Warrick**[1,2], **Daniel M Neumark**[1,2] **and Stephen R Leone**[1,2,3]

[1] Chemical Sciences Division, Lawrence Berkeley National Laboratory, Berkeley, CA 94720, USA
[2] Department of Chemistry, University of California, Berkeley, CA 94720, USA
[3] Department of Physics, University of California, Berkeley, CA 94720, USA

E-mail: caowei1688@gmail.com

Keywords: attosecond transient absorption, population transfer, Stark shift, Rydberg states

Abstract

Using attosecond transient absorption, the dipole response of an argon atom in the vacuum ultraviolet (VUV) region is studied when an external electromagnetic field is present. An isolated attosecond VUV pulse populates Rydberg states lying 15 eV above the argon ground state. A synchronized few-cycle near infrared (NIR) pulse modifies the oscillating dipoles of argon impulsively, leading to alterations in the VUV absorption spectra. As the NIR pulse is delayed with respect to the VUV pulse, multiple features in the absorption profile emerge simultaneously including line broadening, sideband structure, sub-cycle fast modulations, and 5–10 fs slow modulations. These features indicate the coexistence of two general processes of the light–matter interaction: the energy shift of individual atomic levels and coherent population transfer between atomic eigenstates, revealing coherent superpositions. An intuitive formula is derived to treat both effects in a unifying framework, allowing one to identify and quantify the two processes in a single absorption spectrogram.

Recently, attosecond transient absorption (ATA) spectroscopy has demonstrated great success in accessing ultrafast dynamics of bound and autoionizing systems in rare gas atoms [1–10] and diatomic molecules [11–13]. In this technique, dipole allowed states (bright states) are coherently populated by a broadband attosecond pulse, forming a wavepacket. The coherence between each individual excited state and the initial ground state forms a polarization dipole. Upon the arrival of a delayed short near infrared (NIR) pulse, these dipoles are subject to a complex amplitude change that occurs within a few femtoseconds, leading to novel absorption features in the transmitted spectrum of the attosecond pulse. Various dynamical aspects of the initially launched wavepacket are imprinted in the delay-dependent absorption spectra. Thus far, ATA studies have generally been carried out at photon energies ranging from 20 to 100 eV due to more efficient high harmonic generation above 20 eV. Here, we report ATA experiments on Ar atoms at photon energies around 15 eV, enabling a detailed study of electronic wavepacket dynamics for Rydberg states approaching the first ionization threshold of Ar.

There are two major effects of the NIR pulse in ATA experiments. First, it shifts the energy of the individual states, generally known as the ac Stark shift. Secondly, it transfers population between different bright states by a two photon process. How these two effects manifest themselves in an ATA measurement is the essence of understanding the observables in such an experiment. The ac Stark shift corresponds to the energy difference between a dressed energy level and its field-free counterpart. In the time domain, it originates from the extra phase modulation, introduced by the NIR field, on the states of interest. The ac Stark shift manifests itself as reshaping of the absorption line profile in an ATA experiment [14, 15]. On the other hand, population transfer between different bright states is generally accomplished by a two or more photon transition mediated by available dark states. The amplitude of a bright state therefore consists of the original portion initiated by the attosecond pulse and the extra portion transferred from other bright states by the NIR pulse. The interference between these two contributions gives rise to periodic modulations on the absorption lines as a function of the

arrival time of the IR pulse. Depending on the position of the dark state, the transition can be the ladder type, where the coupled dark state is situated between the two bright states, corresponding to sub-cycle modulation features [5, 9–13, 16–18], or a vee (lambda) type wherein the dark state is on the same side above (below) the two bright states in energy [19], corresponding to a slower modulation period in the absorption lines [6]. Therefore, the periodic modulation of the amplitude of a particular absorption line is generally recognized as the signature of population transfer.

These two effects have been demonstrated for many atomic systems mostly in a qualitative way [6, 9–13, 16, 17]. Recent quantitative studies on helium atoms emphasize either the dynamic Stark shift of bound states [14, 15] or resonant population transfer between doubly excited states [4, 20]. In this work, we perform ATA on argon atoms in the VUV region, where high lying Rydberg states of argon close to the first ionization threshold are active. Both Stark shift and population transfer processes are found to play equally important roles in this energy range, giving rise to abundant transient absorption features such as line broadening, sideband structure, sub-cycle fast modulations, and 5–10 femtosecond slow modulations. An intuitive model is derived to treat both effects in a unifying framework, allowing us to identify and quantify the two processes simultaneously.

In this experiment, double optical gating (DOG) [21] is applied to shape a 6 fs near NIR driving pulse (HE CEP, Femtolasers) for high order harmonic generation in xenon gas. By using a 200 nm indium filter, a continuous spectrum in the VUV region around 15 eV is obtained. The spectrum spans 14.5–16.5 eV with a weak tail extending to as low as 11 eV, supporting a transform limited pulse duration of about 500 as. Under similar experimental conditions, the attosecond pulses were characterized [22] using the FROG–CRAB technique [23], which indicated that the actual pulse duration is slightly longer than that of the transform limited pulse considering the intrinsic chirp of the as pulse and the dispersion of the gas medium for high order harmonic generation. This VUV attosecond pulse is focused with a toroidal mirror into a 1 mm cell filled with a few torr (a few hundred Pascal) of argon gas. A replica of the NIR pulse centered around 780 nm is picked off by a beamsplitter and combined with the attosecond pulse using an annular mirror before the target cell. The relative delay of the VUV and NIR pulses is controlled by a piezoelectric-transducer delay stage with ~100 as time resolution. After interacting with the target gas in the cell, the transmitted VUV spectrum is dispersed with a high resolution (15 meV around 20 eV) flat-field grating (Hitachi 001-0464) and recorded by a CCD camera (Pixis XO 400B, Princeton Instruments).

Figure 1 shows the delay dependent absorption spectra of argon with positive delays indicating that the VUV pulse precedes the NIR probe pulse. The intensity of the NIR pulse, 5×10^{12} W cm^{-2}, is estimated based on its focusing geometry. The VUV photon promotes a 3p valence electron into the Rydberg series $3s^23p^6 \rightarrow 3s^23p^5[^2P_{1/2,3/2}]nd(s)$. Two groups of ns/nd manifolds converging to different spin–orbit coupled ion core limits, $I_{P[3/2]} = 15.76$ eV and $I_{P[1/2]} = 15.94$ eV, are populated. The valence electronic wavepacket initiated by the VUV pulse experiences an electromagnetic interaction upon the arrival of the NIR pulse. There are four distinct effects attributable to the NIR pulse, each of which is labelled in figure 1. (a) It broadens/shifts individual absorption lines at small positive delays. (b) Horizontal sideband structures between two adjacent absorption resonances develop at large positive delays. (c) Fast modulations with a period of 1.3 fs appear on the two 4d states lying around 15 eV. (d) Slow modulations with a period of 5–10 fs appear on the states approaching the ionization limits (~15.75 eV). The coexistence of all four of these very different absorption features has not been observed in previous ATA experiments. Features (a) and (b) are due to the ac Stark shift. Feature (a) has been recognized in previous work as a consequence of the impulsive phase shift induced by the short NIR pulse [14, 15]. Feature (b) stems from the interplay between the hyperbolic lines (perturbed free induction decays) originating from two adjacent resonance states and can be used to quantify the ac Stark shift. Features (c) and (d) are due to population transfer, and they correspond to the ladder-type [5, 9–13, 16–18] and vee-type transition schemes [6], respectively. The identification of all these features is based on the following model calculation.

The minimal requirement to depict the ATA experiment qualitatively is a four level system: an initial ground state $|g\rangle$, two bright states $|1\rangle$, $|2\rangle$ forming the simplest wavepacket, and a dark state $|3\rangle$ that couples with the bright states in the presence of the NIR pulse. Assume that the attosecond pulse at $t = 0$ launches a wavepacket $\Psi(t = 0) = \sum_n c_n(0)|n\rangle$, $n = 1, 2$, where the coefficients $c_n(0)$ are the initial complex amplitudes of state $|n\rangle$ and the amplitude of the ground state remains unchanged. The excited state wavepacket evolves in time according to (atomic units throughout):

$$\begin{pmatrix} c_1(t) \\ c_2(t) \\ c_3(t) \end{pmatrix} = \hat{T} e^{-i\int_0^t [H_0 + V(t')]dt'} \begin{pmatrix} c_1(0) \\ c_2(0) \\ c_3(0) \end{pmatrix}, \quad (1)$$

where H_0 is the field free Hamiltonian,V(t) is the interaction with the NIR pulse, and $\hat{T}$ is the time ordering operator. The solutions that describe the system evolution starting from a single state after the attosecond pulse excitation, taking into account that only bright states are initially populated, are:

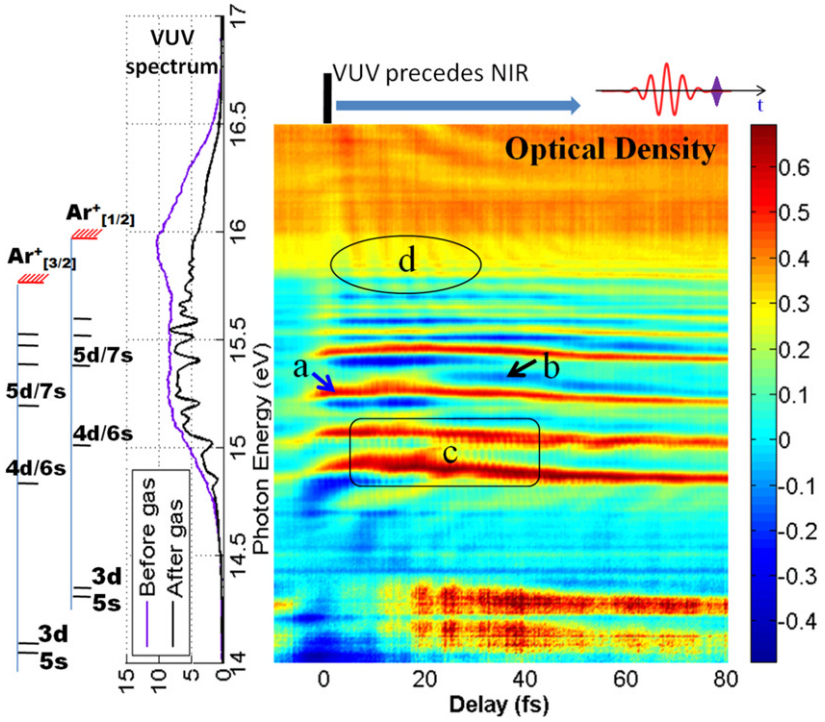

Figure 1. The measured delay dependent absorption spectra of argon in terms of optical density (OD): $-\log_{10}\left(\frac{I_t}{I_0}\right)$, where I_0 and I_t are the spectral densities before and after the gas cell, respectively. The VUV spectrum below 14.5 eV decreases quickly down to the noise level and thus the OD below 14.5 eV is not reliable. Labels a–d indicate the four types of absorption features identified, see text for the details.

$$\begin{pmatrix} A_1^1(t) \\ A_1^2(t) \\ A_1^3(t) \end{pmatrix} = \hat{T} e^{-i\int_0^t [H_0+V(t')]dt'} \begin{pmatrix} 1 \\ 0 \\ 0 \end{pmatrix} \tag{2}$$

$$\begin{pmatrix} A_2^1(t) \\ A_2^2(t) \\ A_2^3(t) \end{pmatrix} = \hat{T} e^{-i\int_0^t [H_0+V(t')]dt'} \begin{pmatrix} 0 \\ 1 \\ 0 \end{pmatrix}. \tag{3}$$

The complex amplitudes for a delayed interaction $V(t_d)$, $t_d = t - \tau$, are:

$$\begin{pmatrix} c_1(t_d) \\ c_2(t_d) \end{pmatrix} = c_1(0) e^{-iE_1\tau} \begin{pmatrix} A_1^1(t_d) \\ A_1^2(t_d) \end{pmatrix} + c_2(0) e^{-iE_2\tau} \begin{pmatrix} A_2^1(t_d) \\ A_2^2(t_d) \end{pmatrix}. \tag{4}$$

E_n specifies the energy of state $|n\rangle$ and τ is the relative delay between the NIR pulse and the attosecond pulse. Here we only consider the amplitude evolution of the bright states $|1\rangle$, $|2\rangle$ that contribute to the dipole radiation. The amplitude of the bright state $|1\rangle$ is then:

$$c_1(t-\tau) = e^{-iE_1\tau}[c_1(0)A_1^1(t-\tau) + c_2(0)A_2^1(t-\tau)e^{-i(E_2-E_1)\tau}]. \tag{5}$$

Note that both the complex amplitudes $A_1^1(t)$ and $A_2^1(t)$ contain a phase term e^{-iE_1t} and the initial amplitude $c_n(0)$ is proportional to the dipole matrix element μ_{ng} between state $|n\rangle$ and the ground state, assuming a uniform spectral distribution of the attosecond pulse in the energy range of interest. A general form of the dipole moment between $|1\rangle$ and the ground state $|g\rangle$ becomes:

$$\begin{aligned} d_1(t) &= -ic_1(t_d)^* <1\ |r|\ g> + cc \\ &\propto \mu_{1g}{}^2 \left[|A_1^1(t-\tau)| \sin(E_1t + \Phi_{A_1^1}) + \frac{\mu_{2g}}{\mu_{1g}} |A_2^1(t-\tau)| \sin(E_1t + \Phi_{A_2^1} + \Delta E_{21}\tau) \right]. \end{aligned} \tag{6}$$

Here $\Delta E_{21} = E_2 - E_1$, and the imaginary unit i in front of $c_1(t_d)^*$ accounts for the attosecond pulse excitation induced phase. $\Phi_{A_1^1}, \Phi_{A_2^1}$ represent the phases of $A_1^1(t-\tau)$ and $A_2^1(t-\tau)$ after factoring out the fast oscillation term $e^{-iE_1(t-\tau)}$. Although equation (6) is derived assuming only two bright states, it can be generalized to a multi-level wavepacket including all the states that give rise to non-negligible contributions:

$$d_1(t) \propto \mu_{1g}{}^2\left[|A_1^1(t-\tau)|\sin(E_1 t + \Phi_{A_1^1}) + \sum_n \frac{\mu_{ng}}{\mu_{1g}}|A_n^1(t-\tau)|\sin(E_1 t + \Phi_{A_n^1} + \Delta E_{n1}\tau)\right],\ n \neq 1. \quad (7)$$

Assuming the dilute gas target behaves approximately as a linear medium, which means that in the frequency domain the polarization $P(\omega)$ of the gas has a linear relationship with the incident electromagnetic field $E(\omega)$, Beer's Law should hold. This assumption is justified because previous studies of transient absorption in helium demonstrated that noticeable distortions of the absorption profile induced by propagation effects mainly occur, in the case of helium, in the vicinity of the low lying 1s2p excited state of helium with a binding energy of about 3.5 eV; for Rydberg states with primary quantum numbers $n > 2$ the propagation effect is strongly suppressed [24, 25]. In our experiment on argon, we focused on the Rydberg series close to the first ionization threshold (binding energy less than 0.7 eV) and thus do not expect significant propagation effects. Therefore the absorption spectrum in terms of optical density will be proportional to the imaginary part of the Fourier transformation of the time dependent dipole moment $d_1(t)$ [26, 27].

Equation (7) formally describes the observables of an ATA experiment in a non-perturbative way. The various terms in equation (7) have clear physical significance. The first sinusoidal term indicates a transition process in which the final and original states coincide, which is mainly a Stark shift term. $|A_1^1(t-\tau)|$ quantifies the laser induced depopulation of state $|1\rangle$, which is generally attributed to ionization or resonant coupling into a dark state. $\Phi_{A_1^1}$ is the phase corresponding to the energy shift of $|1\rangle$. The second term in the expression indicates a transition in which the final and original bright states are different, a population transfer term. $|A_n^1(t-\tau)|$ is the population transfer magnitude from $|n\rangle$ to $|1\rangle$. This term contains a delay dependent phase $\Delta E_{n1}\tau$, which specifies a measurable time constant of the coherent superposition wavepacket consisting of the two states $|1\rangle$ and $|n\rangle$. In the case of a short, few cycle NIR pulse, the onset of $\Phi_{A_1^1}$ and $|A_n^1(t-\tau)|$ occurs promptly and approximately follows the time integral of the laser intensity envelope. Equation (7) in principle can fully characterize the ATA experiments, given the values of $A_1^1(t)$ and $A_n^1(t)$. The exact forms of $A_1^1(t)$ and $A_n^1(t)$ are generally inaccessible for arbitrary complex atomic systems due to the lack of accurate information of the atomic structure. However, equation (7) phenomenologically decouples the two effects, and effectively reveals the direct competition between them. A comparison with the experimental results potentially allows a quantification of the contribution of each effect. The second term of equation (7) results from the coherent nature of the wavepacket prepared by the broadband VUV pump pulse; a precise control of the delay will allow effective control of the inter-level population transfer. On the other hand, if the pump pulse has a well defined frequency at the expense of temporal resolution, a particular electronic state can be singled out to emphasize the physical processes governed by the first term of equation (7) such as electromagnetically induced transparency and Autler–Townes splitting [28].

With the help of the first term in equation (7), we can reassemble the absorption spectrogram pattern that is caused only by the energy shift effect. Most of the states of interest are loosely bound high-lying Rydberg states, for which the energy shift approaches the energy of a classical electron in an electromagnetic field: $\varepsilon(t)\cos(\omega_0 t)$, where $\varepsilon(t)$ and ω_0 denote the envelope and the central angular frequency of the laser field, respectively. The instantaneous energy shift is: $\delta \mathrm{E}(t) = \frac{1}{2}\int_{-\infty}^{t}[\varepsilon(t')\cos(\omega_0 t')]^2\,\mathrm{d}t' \approx \frac{\varepsilon(t)^2}{2\omega_0^2}$, and thus it is legitimate to evaluate the related phase in equation (7), $\Phi_{A_n^n(t)} = \int_0^{\mathrm{t}}\delta \mathrm{E}(t')\mathrm{d}t'$, which solely depends on the laser parameters. The depopulation factor $|A_n^n(t)|$ is approximately equal to unity due to the assumptions that the coupling between Rydberg states and continuum states (ionization) is weak and Rabi-cycling into a dark state is generally much slower than the few cycle laser pulse duration. Figure 2 shows the calculated results when only the first sinusoidal term in equation (7) is considered. At delay $\tau = 0$, the radiation dipole for each individual state gains a rapid increasing phase term from the laser field. This is analogous to asymmetric nonlinear self phase modulation and will broaden the absorption line as shown in figure 2(a). The phase imposed by the NIR pulse changes the absorption profile from Lorentzian to Fano, similar to previous studies [14, 15]. To understand the role of the laser-imposed phase in the absorption spectra, we evaluate the optical density for an oscillating dipole with the form: $\mathrm{d}(t) = \mathrm{e}^{-t/\Gamma}\sin[\omega_0 t + \varphi(t > \tau)]$, where ω_0 is the energy difference between the ground and excited state, Γ is the lifetime of the excited state, and $\varphi(t > \tau)$ specifies the laser-imposed phase when the IR pulse arrives at time τ. The Fourier transform of the dipole is:

$$\tilde{d}(\omega) = \int_0^\infty \mathrm{d}(t)\mathrm{e}^{-\mathrm{i}\omega \mathrm{t}}\mathrm{d}t = \int_0^\infty \mathrm{e}^{-\frac{t}{\Gamma}}\sin(\omega_0 \mathrm{t})\mathrm{e}^{-\mathrm{i}\omega t}\mathrm{d}t + \int_\tau^\infty \mathrm{e}^{-\frac{t}{\Gamma}}[\sin(\omega_0 t + \varphi) - \sin(\omega_0 t)]\mathrm{e}^{-\mathrm{i}\omega t}\mathrm{d}t. \quad (8)$$

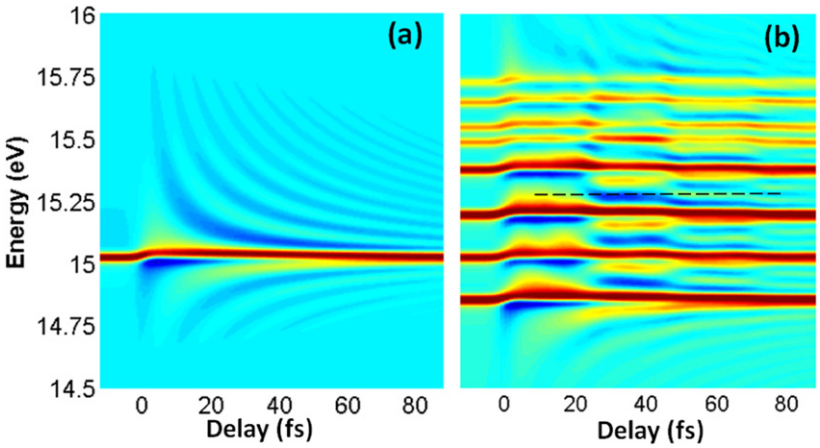

Figure 2. Simulated absorption spectrogram for a single radiation dipole (a) and multiple radiation dipoles (b). The population transfer term is ignored in this calculation, i.e. $|A_n^m\ (t > \tau)| = 0,\ \ m \neq n$. The spectrum at each delay is calculated as the imaginary part of $\tilde{d}_m(\omega)$, where $\tilde{d}_m(\omega) = \sum_n \int_0^\infty d_m(t)\mathrm{e}^{-\mathrm{i}\omega t}\mathrm{d}t$ is the Fourier transform of the dipole moment from equation (7), and then convoluted with a Gaussian function with a width of 15 meV to include the instrumental resolution. The 780 nm NIR pulse has a peak intensity of 3.5×10^{12} W cm^{-2} and a pulse duration of 6 fs. The dipole matrix elements used in the calculation are adopted and tabulated from [29]. The eight energy levels (14.85 eV, 15.02 eV, 15.189 eV, 15.37 eV, 15.48 eV, 15.54 eV, 15.64 eV, 15.72 eV) in the calculation are chosen based on the major absorption features in figure 1.

Define the free decay term as:

$$\int_0^\infty \mathrm{e}^{-\frac{t}{\Gamma}}\sin(\omega_0 t+\phi)\mathrm{e}^{-\mathrm{i}\omega t}\mathrm{d}t = \int_0^\infty \mathrm{e}^{-\frac{t}{\Gamma}}\frac{\mathrm{e}^{\mathrm{i}(\omega_0 t+\phi)}}{2i}\mathrm{e}^{-\mathrm{i}\omega t}\mathrm{d}t = \frac{\mathrm{e}^{\mathrm{i}\phi}}{2\mathrm{i}\left[\frac{1}{\Gamma}+\mathrm{i}(\omega-\omega_0)\right]} = \mathrm{e}^{\mathrm{i}\phi}\mathrm{F}(\omega),\ \ \omega>0. \tag{9}$$

Then equation (8) is:

$$\begin{aligned}\tilde{d}(\omega) &= F(\omega) + 2\cdot\ \sin\frac{\varphi}{2}\int_\tau^\infty \mathrm{e}^{-\frac{t}{\Gamma}}\cos\left(\omega_0 t+\frac{\varphi}{2}\right)\mathrm{e}^{-\mathrm{i}\omega t}\mathrm{d}t\\ &= F(\omega) + 2\cdot\ \sin\frac{\varphi}{2}\cdot\mathrm{e}^{-\frac{\tau}{\Gamma}}\cdot\mathrm{e}^{-\mathrm{i}\omega\tau}\int_0^\infty \mathrm{e}^{-\frac{t}{\Gamma}}\sin\left(\omega_0 t+\frac{\varphi}{2}+\omega_0\tau+\frac{\pi}{2}\right)\mathrm{e}^{-\mathrm{i}\omega t}\mathrm{d}t\\ &= F(\omega) + 2\cdot\ \sin\frac{\varphi}{2}\cdot\mathrm{e}^{-\frac{\tau}{\Gamma}}\cdot\mathrm{e}^{-\mathrm{i}\omega\tau}\mathrm{e}^{\mathrm{i}\left(\frac{\varphi}{2}+\omega_0\tau+\frac{\pi}{2}\right)}F(\omega)\\ &= F(\omega)\left\{1+2\cdot\ \sin\frac{\varphi}{2}\cdot\mathrm{e}^{-\frac{\tau}{\Gamma}}\mathrm{e}^{\mathrm{i}\left[(\omega_0-\omega)\tau+\frac{\varphi}{2}+\frac{\pi}{2}\right]}\right\}.\end{aligned} \tag{10}$$

For long lived bound states, we assume: $|\omega-\omega_0| \gg \frac{1}{\Gamma}$, then $F(\omega) \propto \frac{1}{\omega_0-\omega}$

$$\tilde{d}(\omega) \propto \frac{1}{\omega_0-\omega}\left\{1+2\cdot\ \sin\frac{\varphi}{2}\cdot\mathrm{e}^{-\frac{\tau}{\Gamma}}\mathrm{e}^{\mathrm{i}\left[(\omega-\omega_0)\tau+\frac{\varphi}{2}+\frac{\pi}{2}\right]}\right\}. \tag{11}$$

The optical density will be proportional to:

$$-\mathrm{Im}[\tilde{d}(\omega)] \propto \frac{\cos\left[(\omega-\omega_0)\tau+\frac{\varphi}{2}\right]}{\omega-\omega_0}\sin\frac{\varphi}{2}\cdot\mathrm{e}^{-\frac{\tau}{\Gamma}}. \tag{12}$$

Equation (12) clearly shows the hyperbolic line structure governed by the term $(\omega-\omega_0)\tau$ in the vicinity of the energy level as the delay increases; the phase of the oscillation as a function of delay for a given frequency is directly related to the laser imposed phase φ. Similar features were reported in transient absorption studies of both semiconductors [30, 31] and gas-phase targets [16, 18, 24].

When multiple bright states are included, the interplay between adjacent states leads to horizontal sidebands as shown in figure 2(b). This is feature (b) that we identified in the experimental data in figure 1. The simulation in figure 2(b) qualitatively recovers a major part of the 'absorption broadening' features in the experimental results, which is attributed to the laser-induced Stark shift. The next question is how to quantify the energy shift. Ott *et al* [15] showed that the absorption line shape is directly linked to the phase (or the product of the energy shift and the pulse duration) introduced by the NIR pulse, thus allowing one to retrieve the Stark shift by fitting the absorption line shape with the theoretical prediction at small delays. However, for a series of Rydberg states

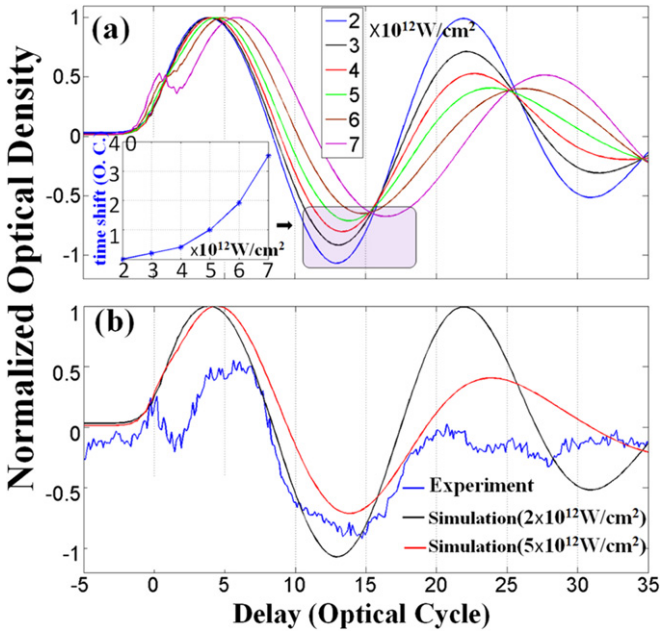

Figure 3. Normalized optical density of the sideband (~15.3 eV) as a function of delay. (a) The simulated results using equation (7) including only the two states lying just above and below this sideband. The inset shows the relative time shift in units of optical cycles of the first valley (purple box) of the oscillation as a function of the laser peak intensity. The time shift is set to be zero for the lowest intensity (2×10^{12} W cm^{-2}). The 780 nm Gaussian laser pulse has a full width at half maximum laser of 6 fs in the calculation. (b) The measured sideband oscillation (blue) compared with the calculated result (black). The peak intensity in the experiment is estimated to be (3.5 ± 1.5) $\times 10^{12}$ W cm^{-2}.

closely spaced in energy, the energy shift can exceed the energy spacing of two adjacent states, making it difficult to trace the absorption line shape. Here, we use an alternative means to quantify the Stark shift. The VUV pulse populates the excited states and each excited state can form a quasi-monochromatic oscillating dipole, the hyperbolic lines coming from different resonant states as shown by equation (12) can interfere, similar to a double-slit interference experiment, resulting in the horizontal sidebands. We can follow the periodic oscillation of a particular sideband along the delay axis. The phase of this oscillation is directly linked with the phase shift induced by the NIR pulse. Figure 3(a) shows the simulated optical density of the sideband around 15.3 eV (indicated by the black dashed line in figure 2(b)) as a function of delay for different laser intensities. The inset in figure 3(a) shows the relative time shift of the first valley in the oscillation (indicated by the purple box) as a function of laser peak intensity. Therefore, the laser intensity (or the Stark shift), is directly mapped onto the oscillation phase of a particular sideband. This mapping process allows us to retrieve the phase that is imposed onto the states by the NIR field.

Figure 3(b) shows the measured sideband oscillation (indicated by the black arrow in figure 1) compared with the simulated results. The two simulated curves indicate the lower and upper limits of the laser peak intensity. The comparison in figure 3(b) suggests that the laser peak intensity in the experiment is (3.5 ± 1.5) $\times 10^{12}$ W cm^{-2}, which is lower than the laser intensity estimated according to the laser focusing geometry. This laser intensity corresponds to a ponderomotive energy shift of 0.20 ± 0.09 eV for the Rydberg states. The discrepancy between the experimental and simulated results is possibly due to the non-uniform intensity distribution in the interaction region as well as the non-Gaussian shape of the NIR pulse used in the experiment. Note that the choice of the sideband is completely arbitrary. As long as the experimental resolution allows, other sidebands can be traced as well to gain quantitative information for the laser induced Stark shift. Although the overall oscillatory behavior in the experimental data is well reproduced by simulation in figure 3, we also notice that the experimental data (blue line in figure 3(b)) reveals relatively weak fast oscillations on top of the regular slow oscillation. Given that only the first sinusoidal term in equation (7) is included in the simulation, we attribute these fast oscillating components to the population transfer processes (second sinusoidal term in equation (7)) that have been neglected in the simulation.

A typical ac Stark shift normally refers to a cycle averaged energy shift of a particular state induced by a monochromatic electric field. When a short laser pulse containing a few cycles is applied, the definition of cycle averaged energy shift breaks down due to the rapid change of the field intensity from one cycle to another, and the energy levels of interest will instead experience a time dependent energy shift following the intensity envelope of the laser field. The uncertainty of this shift is governed by the time-energy relationship. In the limit

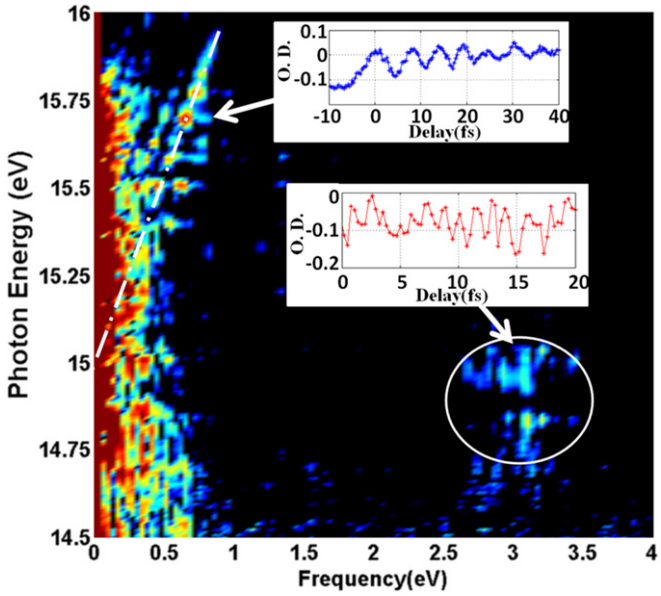

Figure 4. Fourier analysis of figure 1 in logarithmic scale. The insets show the delay dependent optical density for two different resonant energy levels, corresponding to slow (blue) and fast (red) modulation components.

of an infinitely long pulse, the Stark shift is reduced to the cycle-averaged energy shift and thus has a well defined value; in the case of a short pulse, the energy shift has a distribution with a width inversely proportional to the pulse duration. Therefore, the estimated Stark shift retrieved from the current experiment only reflects the energy shift averaged over the entire temporal span of the NIR pulse. Although the short pulse cannot implement a precise control on the energy structure of a quantum system, it can promptly impose a phase onto a particular state with a precise timing, allowing an effective control of the absorption line profile in the light–matter interaction.

Apart from the absorption features due to a Stark shift just discussed, absorption features due to the population transfer effect, identified as features (c) and (d) in figure 1, can also be reproduced with the help of equation (7). The second sinusoidal term of equation (7) suggests that the absorption strength of a particular resonant state $|1\rangle$ oscillates at a frequency corresponding to the energy difference ΔE_{n1}. To accurately identify the involved states that are participating in the population transfer process, a Fourier analysis of figure1 with respect to the delay axis is performed and the results are shown in figure 4. The fast modulations (circle in figure 4) have a frequency corresponding to an energy of 3.2 eV, approximately twice the photon energy of the 780 nm NIR pulse. According to equation (7), this modulation results from the NIR assisted population transfer from a low lying bright state situated around 11.8 eV, and we identify the $[^2P_{1/2,3/2}]4s$ (~11.8 eV) states to be the best candidates. In order to observe noticeable population transfer amplitude, a dark state needs to be resonantly coupled to the two bright states by the NIR photon. As shown in figure 5, the 4*p* manifold in Ar, which includes 4 states that fulfill the selection rule, appears around 13.3 eV and serves as the near resonant intermediate states in this experiment. Such a fast modulation is a result of a ladder scheme population transfer with the resonant dark state sitting between the $[^2P_{1/2,3/2}]4s$ (~11.8 eV) and $[^2P_{1/2}]4d/6s$ (~15 eV) bright states (see figure 5 for the transition pathway). This scheme gives rise to a modulation period (1.3 fs) that corresponds to an energy equal to the addition of the two photon energies (~1.5 and ~1.7 eV) for coupling.

As shown in figure 4, the slower modulations have dominant frequency components that line up precisely along the white dashed line with slope equal to 1 in figure 4. This line intersects with the vertical axis at 15 eV (the $[^2P_{1/2}]4d/6s$ state), indicating a NIR assisted population transfer process from $[^2P_{1/2}]4d/6s$ to Rydberg states close to the ionization threshold following equation (7). With the same 4p manifold (~13.3 eV) as the near resonant dark states, this slower modulation case corresponds to a vee scheme population transfer, in which the $[^2P_{1/2}]4d/6s$ (~15 eV) state is resonantly coupled downwards with 4p using a redder photon (~1.7 eV) and the 4p then couples upwards with Rydberg states with a bluer photon (~2.4 eV); see figure 5 for the transition pathway. This scheme leads to a modulation frequency (5–10 fs) equal to the energy difference of the redder and bluer photons. Weaker modulation frequency components near the white dashed line in figure 4 also tend to line up along lines with slope unity. They result from NIR assisted vee type population transfer from other states ($[^2P_{3/2}]5d/7s$ at 15.19 eV and $[^2P_{3/2}]4d/6s$ at 14.85 eV) to the upper Rydberg states, with a relatively lower

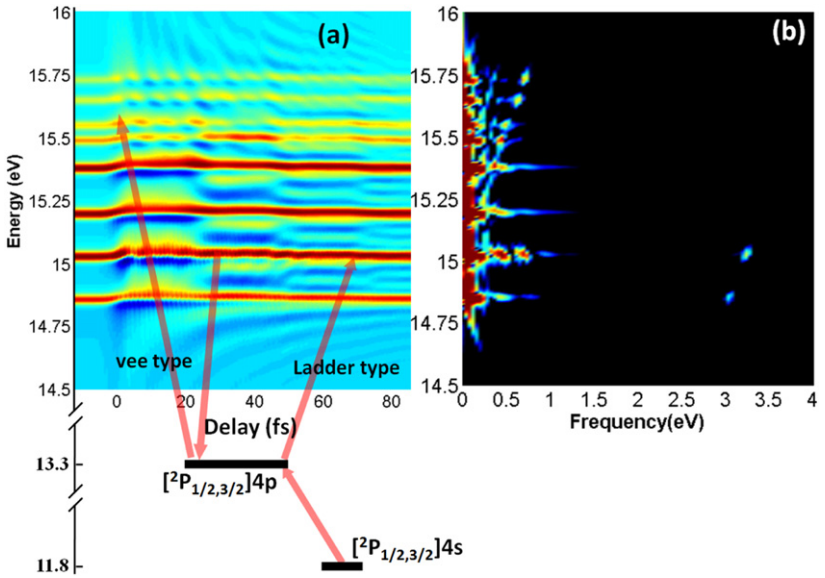

Figure 5. Simulated absorption spectrogram for eight resonance states. Both the energy shift term and population transfer term in equation (7) are considered. The spectrum at each delay is calculated using the same method and laser parameters as figure 2. The mutual population transfer amplitudes $|A_n^m\ (t > \tau)|$ from $[^2P_{1/2}]4d/6s$ (15 eV) to the other seven states (low to high energy order, lambda transfer scheme) are: 0.1, 0.1, 0.05, 0.15, 0.15, 0.2, 0.2, the amplitude change of states situated at 14.85 and 15 eV due to ladder scheme transfer from $[^2P_{1/2}]4s$ (11.8 eV) is assumed to be 0.1. Phases $\phi_{A_n^m}$ are zero. The arrows show the two identified population transfer schemes.

probability compared to the ones labeled with the white dashed line. The spectrum of the 6 fs NIR pulse used in the experiment spans 500 nm (~2.48 eV) to 900 nm (~1.38 eV) , which covers the photon energies needed in the two proposed transfer schemes mentioned above.

In principle, the population transfer amplitude after the laser pulse $|A_n^1(t > \tau)|$ can be directly read off from the experimental measurement if the modulation depth can be extracted accurately. Ideally, the modulation depth corresponding to a certain state is the ratio between the amplitude of the modulation frequency of interest and that of the dc component. However, due to limited frequency resolution and inevitable slow experimental fluctuations, the modulation depth estimated from the Fourier analysis in figure 4 is generally underestimated. To reconstruct the dominant modulation features in figure 1, we can estimate the amplitude $|A_n^1(t > \tau)|$ and phase $\Phi_{A_n^1}$ directly from the delay dependent optical density at small delays (the insets of figure 3); here the amplitude is retrieved from the modulation depth $\frac{\mu_{1g}\,|\,A_n^1(t>\tau)\,|}{\mu_{ng}\,|\,A_1^1(t>\tau)\,|}$ assuming $|A_1^1(t > \tau)|$ is close to unity. The simulation based on equation (7) including both sinusoidal terms is shown in figure 5. For the slower modulations (dashed line in figure 4), we only consider the mutual population transfer between $[^2P_{1/2}]4d/6s$ (15.02 eV) and other states lying at 14.85 eV, 15.189 eV, 15.37 eV, 15.48 eV, 15.54 eV, 15.64 eV and 15.72 eV, which is the dominant process according to figure 4. The population transfer amplitudes $|A_n^m\ (t > \tau)|$ are determined to be 0.1, 0.1, 0.05, 0.15, 0.15, 0.2 and 0.2, respectively. For the fast modulation (circle in figure 4), the amplitude change of the state $[^2P_{1/2}]4d/6s$ (15.02 eV) due to ladder scheme transfer from $[^2P_{1/2}]4s$ (11.8 eV) is assumed to be 0.1.

By considering the two possible population transfer schemes discussed above, the experimental observations in figure 1 are remarkably well-reproduced by the model. This suggests that both energy shifts and population transfer play important roles in the argon experiment in this region, and manifest themselves as different absorption patterns. Although the model only considers a single active electron, it still captures the major processes of the experiment, thus indicating that the single electron response is still dominant. Furthermore, this experiment shows the difference between the ATA spectrum of complex atomic systems, such as argon, and that of a simpler atomic system, helium. Unlike helium, where a ladder type population transfer usually dominates the absorption spectrum in the Rydberg series (corresponding to sub-cycle modulations), the argon transient absorption spectrum shows clear vee type population transfer features. This may be attributed to the very different atomic structure and dipole matrix elements, which can be explored in future studies.

In conclusion, the dipole response of an argon atom in the VUV region to an external electromagnetic field has been studied using ATA spectroscopy. Both Stark shift and population transfer effects play important roles in the absorption spectra, giving rise to complex absorption features such as the line broadening, sideband structure, sub-cycle fast modulations, and 5–10 fs slow modulations. With the help of an intuitive model that

treats both effects in a distinguishable way, we successfully identified and quantified the absorption features that are attributed to different effects. It reveals that the combined effects are essentially general phenomena in ATA experiments of atomic targets and thus have to be treated on equal footing. While the effects seen here have been previously observed in different contexts, this study shows how they are manifested and interpreted in ATA experiments. It thus provides a foundation for understanding ATA of more complex systems, particularly small molecules in which additional spectroscopic and dynamical features associated with vibrational motion and predissociation are expected.

Acknowledgments

This work was supported by the Director, Office of Science, Office of Basic Energy Sciences and by the Division of Chemical Sciences, Geosciences, and Biosciences of the US Department of Energy at LBNL under contract no. DE-AC02-05CH11231.

References

[1] Wang H, Chini M, Chen S, Zhang C H, He F, Cheng Y, Wu Y, Thumm U and Chang Z 2010 *Phys. Rev. Lett.* **105** 143002
[2] Bernhardt B, Beck A R, Li X, Warrick E R, Bell M J, Haxton D J, McCurdy C W, Neumark D M and Leone S R 2014 *Phys. Rev.* A **89** 023408
[3] Chini M, Zhao B, Wang H, Cheng Y, Hu S and Chang Z 2012 *Phys. Rev. Lett.* **109** 073601
[4] Kaldun A, Ott C, Blattermann A, Laux M, Meyer K, Ding T, Fischer A and Pfeifer T 2014 *Phys. Rev. Lett.* **112** 103001
[5] Ott C *et al* 2014 *Nature* **516** 374
[6] Beck A R, Bernhardt B, Warrick E R, Wu M, Chen S, Gaarde M B, Schafer K J, Neumark D M and Leone S R 2014 *New J. Phys.* **16** 113016
[7] Beck A R, Neumark D M and Leone S R 2015 *Chem. Phys. Lett.* **624** 119
[8] Li X, Bernhardt B, Beck A R, Warrick E R, Pfeiffer A N, Bell M J, Haxton D J, McCurdy C W, Neumark D M and Leone S R 2015 *J. Phys. B: At. Mol. Opt. Phys.* **48** 125601
[9] Lucchini M, Herrmann J, Ludwig A, Locher R, Sabbar M, Gallmann L and Keller U 2013 *New J. Phys.* **15** 103010
[10] Chini M, Wang X, Cheng Y and Chang Z 2014 *J. Phys. B: At. Mol. Opt. Phys.* **47** 124009
[11] Sansone G, Reduzzi M, Dubrouil A, Feng C, Nisoli M, Calegari F, Lin C D, Chu W C, Poletto L and Frassetto F 2013 *CLEO: QELS_Fundamental Science* (Washington, DC: Optical Society of America) pp QF2C–1
[12] Cheng Y, Chini M, Wang X, Wu Y and Chang Z 2014 *CLEO: QELS_Fundamental Science* (Washington, DC: Optical Society of America) pp FM2B–M23
[13] Bækhøj J E, Yue L and Madsen L B 2015 *Phys. Rev.* A **91** 043408
[14] Chen S, Wu M, Gaarde M B and Schafer K J 2013 *Phys. Rev.* A **88** 033409
[15] Ott C, Kaldun A, Raith P, Meyer K, Laux M, Evers J, Keitel C H, Greene C H and Pfeifer T 2013 *Science* **340** 716
[16] Chini M, Wang X, Cheng Y, Wu Y, Zhao D, Telnov D A, Chu S I and Chang Z 2013 *Sci. Rep.* **3** 1105
[17] Wang X, Chini M, Cheng Y, Wu Y, Tong X M and Chang Z 2013 *Phys. Rev.* A **87** 063413
[18] Chen S, Wu M, Gaarde M B and Schafer K J 2013 *Phys. Rev.* A **87** 033408
[19] Fleischhauer M, Imamoglu A and Marangos J P 2005 *Rev. Mod. Phys.* **77** 633
[20] Blattermann A, Ott C, Kaldun A, Ding T and Pfeifer T 2014 *J. Phys. B: At. Mol. Opt. Phys.* **47** 124008
[21] Mashiko H, Gilbertson S, Li C, Khan S D, Shakya M M, Moon E and Chang Z 2008 *Phys. Rev. Lett.* **100** 103906
[22] Mashiko H, Bell M J, Beck A R, Abel M J, Nagel P M, Steiner C P, Robinson J, Neumark D M and Leone S R 2010 *Opt. Express* **18** 25887
[23] Mairesse Y and Quéré F 2005 *Phys. Rev.* A **71** 011401
[24] Pfeiffer A N, Bell M J, Beck A R, Mashiko H, Neumark D M and Leone S R 2013 *Phys. Rev.* A **88** 051402
[25] Liao C T, Sandhu A, Camp S, Schafer K J and Gaarde M B 2015 *Phys. Rev. Lett.* **114** 143002
[26] Santra R, Yakovlev V S, Pfeifer T and Loh Z H 2011 *Phys. Rev.* A **83** 033405
[27] Gaarde M B, Buth C, Tate J L and Schafer K J 2011 *Phys. Rev.* A **83** 013419
[28] Yoshida S, Reinhold C O, Burgdörfer J, Ye S and Dunning F B 2012 *Phys. Rev.* A **86** 043415
[29] Chan W, Cooper G, Guo X, Burton G and Brion C 1992 *Phys. Rev.* A **46** 149
[30] Lindberg M and Koch S W 1988 *Phys. Rev.* B **38** 7607
[31] Sokoloff J P, Joffre M, Fluegel B, Hulin D, Lindberg M, Koch S W, Migus A, Antonetti A and Peyghambarian N 1988 *Phys. Rev.* B **38** 7615